Supplemental Table 1. Crystallographic Analysis of the NFAT1:FOXP3:DNA complex

Table 1 X-ray refinement statistics

Resolution (Å)	50.0-2.80 Å
*R*work/*R*free	24.8%/28.3%
Number of atoms	
Protein	7382
DNA	1712
B-factors	
Protein	60.837 Å2
DNA	60.112 Å2
R.m.s deviations	
Bond lengths (Å)	0.0083
Bond angles (¢X)	1.39

R-factor = Σ ||Fo|-|Fc||/ Σ |Fo| where |Fo| and |Fc| are observed and calculated structure factor amplitudes, respectively. Rfree is calculated for a randomly chosen 8.3% of reflections.

Supplemental Experimental Procedures.

Sample preparation and crystallization

Human FOXP3 (336-419) and NFAT1 RHR (392-678) were prepared as previously described (Stroud et al., 2006; Wu et al., 2006). The DNA fragments used for crystallization and electrophoresis mobility shift assays were synthesized by IDT and purified as described previously (Stroud et al., 2006; Wu et al., 2006). The NFAT1:FOXP3:DNA ternary complex was prepared by mixing purified NFAT1 RHR, the FOXP3 forkhead domain (dimer), and DNA at 1:1:1molar ratio at approximately 12 mg/mL in the buffer: 5 mM HEPES, pH 7.63, 2 mM dithiothreitol (DTT), 0.5 mM EDTA and 150 mM NaCl. Crystals were grown by hanging drop at 18 °C using a reservoir buffer of 50 mM Bis-Tris propane (BTP) (pH 6.65), 6% (w/v) PEG 8000, 104 mM NaCl, 10 mM CaCl2, 5 mM MgCl2, 6% (v/v) glycerol. Crystals belong to the space group $P2_1$ with cell dimensions a=83.667 Å, b=131.234 Å, c=68.665 Å, and β=89.95°.

Data collection, structure determination, and analysis

The NFAT1:FOXP3:DNA complex crystals were stabilized in the harvest/cryoprotectant buffer: 50 mM Bis-Tris propane (BTP) (pH 6.65), 6% (w/v) PEG8000, 104 mM NaCl, and 20% (w/v) glycerol. Data were collected at the ALS BL8.2.1 beam line at the Lawrence Berkeley National Laboratory. Data were reduced using HKL2000 (Otwinowski and Minor, 1997). The crystal diffracted to 2.8Å resolution. The data are 99.2% complete with more than 70% data having average redundancies of 6. The I/sigma for the entire data set (50-2.8Å) and the last bin (2.80-2.93Å) are 35 and 4, respectively. The linear Rmerge for the entire data set (50-2.8Å) and the last bin (2.80-2.93Å) are 5.7% and 45.2%, respectively. Initial phases were determined by molecular replacement using the coordinates of NFAT RHR-N 4and FOXP2 (Stroud et al., 2006). Molecular replacement, refinement and final analysis were done with the software 'CNS' (Crystallography and NMR System) (Brunger et al., 1998). The statistics of crystallographic analysis are presented in Supplemental Table 1. Figures of structure illustration were prepared using MOLSCRIPT (Kraulis, 1991), Ribbons (Carson, 1991) and Pymol (DeLano Scientific). Model building and structural comparisons were carried out in the software 'O' (Jones et al., 1991). The coordinates and structural factors have been deposited in the RCSB protein database under accession code 3QRF.

Chemical cross-linking, site-specific mutagenesis, and multi-angle light scattering analysis

For the chemical cross-linking, various combinations of the NFAT1 RHR (~ 12 μM), the forkhead

domain of FOXP3 (~15 μM monomer) and DNA (ARRE2 or a nonspecific DNA control, ~ 12 μM) were incubated with 2.7 mM disuccinimidyl suberate (DSS) for one hour at room temperature in 20 *μ*l buffer: 25 mM HEPES, pH 7.61, 100 mM NaCl, in 20 *μ*l volumes. At the end of reaction time, 1 *μ*l 1M Tris, pH 7.5, was added to quench the reaction. Samples were then dissolved in denaturing loading dye, analyzed via SDS-PAGE with Coomassie blue staining. Site-specific mutations in FOXP3 were made with QuikChange (Stratagene). The mutants were expressed and purified similarly to the wild type protein (see above). The mutants and the wild type FOXP3 were analyzed by a multi-angle light scattering detector (MALS) (DAWN-EOS, Wyatt Technologies) after separation by a size exclusion column (KW-803, Shodex) on HPLC. A monomeric FOXP2 mutant (Ala539Pro) characterized previously was used as a control in MALS analyses (Stroud et al., 2006).

In-gel FRET Analysis

A long single stranded DNA fragment (5'-CAA GGT AAA CAA GAG CCC CCC CCC CCC AGA GTA AAC AAG TC-3') which contained two optimized FOXP3-binding sites (Koh et al., 2009) was annealed at equal mole to Cy3 labeled DNA (5'-CTC TTG TTT ACC TTG /Cy3/-3') and Cy5 labeled DNA (5'-/Cy5/GAC TTG TTT ACT CT-3'). The resulting probe, labeled at the 5' and 3' ends with the FRET-pair Cy3 and Cy5 respectively, consisted of two double-stranded FOXP3 binding sites separated by a flexible 19-base single-stranded DNA linker. The ability of the dimeric forkhead domain to bring the two FOXP3-binding sites in the synthetic probe described above in close proximity was determined by in-gel FRET analysis. Briefly, the partially paired DNA and FOXP3 (336-419) were mixed in 10μl buffer (10mM Hepes pH 7.6-150mM NaCl-5mM DTT- 10% Glycerol) by keeping DNA concentration of 5μM consistently and titrating with FOXP3 at 0, 0.5, 1, 2, 4, 6, 8 fold of DNA. After 20 min incubation at room temperature, samples was loaded onto 6% TBE gel, which was run in 0.5X TBE buffer with 150 voltages at 4 C. The gel was scanned with a Typhoon 8610 variable mode imager (Amersham Biosciences) at excitation wavelength of 532nm, which excited Cy3, and the fluorescence images were detected at emission wavelength of 580nm for Cy3 and 670nm for Cy5 respectively. The Cy3 image was assigned in green and Cy5 image in red. The two images were overlaid resulting the final image.

Flow cytometry and intracellular staining

T cells were stained intracellularly for IL-2, CTLA-4 and FOXP3 at day 4 after retroviral infection, and cell-surface staining for CD25 and GITR was at day 5 after infection respectively. Intracellular staining for CTLA4 and FOXP3 was performed on unstimulated T cells. Foxp3 expression was found to correlate linearly with Thy1 expression in cells transduced with the retroviral construct MSCV-Foxp3-IRES-Thy1 (data not shown). Hence, Thy1 was utilized as a surrogate marker for Foxp3 expression in experiments evaluating IL-2, GITR and CD25 expression. Intracellular staining for IL-2 was performed after stimulation for 6 hours with PMA (10 nM) and Ionomycin (1 μM). Brefeldin A (10 μg/ml; Sigma) was added during the last 2 hours of stimulation. Cells were washed in PBS-1%BSA, fixed with 4% paraformaldehyde in PBS for 15 min at 25 °C, washed in PBS, and permeabilized in saponin buffer (PBS, 0.5% saponin (Sigma), 1% BSA and 0.1% sodium azide). Nonspecific antibody binding was blocked with Fc block (Pharmingen) before intracellular staining with allophycocyanin-conjugated anti-IL-2 (Ebiosciences), phycoerythrin-anti-CTLA-4 (BD Pharmingen), or phycoerythrin-conjugated anti-FOXP3 (E-biosciences). In some experiments, cell surface staining was completed before fixation. Cells were washed in saponin buffer and in PBS and were analyzed with a FACSCalibur flow cytometer (Becton Dickinson) and FlowJo software. Flow cytometry data are presented as contour plots of IL-2. Numbers in the upper right quadrant indicate the % of $Thy1^{Hi}$ cells expressing IL-2.

Real-time RT-PCR

CD4+ T cells were transduced with the retroviral constructs co-expressing *Thy1.1* marker and WT-*FOXP3* or the domain-swap mutant and expanded either in the absence or presence of 100 Units/ml of recombinant human IL-2. Three days after transduction the cells were stained with phycoerythrin-conjugated anti-Thy1.1 and the transduced cells were sorted based on the expression of cell surface

Thy1.1 by positive selection utilizing anti-PE microbeads (Miltenyi).). Sorted cells were left unstimulated or stimulated for 4 hours with plate-bound anti-CD3 and anti-CD28, and total RNA was prepared using the Trizol reagent (Invitrogen).cDNA was synthesized from total RNA using oligo(dT) primers and Superscript III reverse transcriptase kit (Invitrogen Life Technologies) according to the manufacturer's recommendations. Real-time RT-PCR was performed on a StepOne plus thermal cycler (Applied Biosystems) using Universal Fast SYBR Green reagents (Roche). Similar trends in relative mRNA levels were observed irrespective of whether the cells were expanded in the absence of presence of exogenous IL2 (Data not shown). Specifically, the data presented in Fig. 5C and 5D were generated using cells that were expanded without addition of any exogenous cytokines.

T cell suppression assay

CD4+ T cells transduced with the retroviral constructs co-expressing Thy1.1 marker and WT Foxp3 or the domain swap mutant were sorted as described above and used as suppressors. CD4+ T cells were isolated from spleens and lymph nodes of mice by positive selection using anti-CD4 magnetic beads (Dynal) followed by depletion of CD25+ cells with anti-CD25 microbeads (Miltenyi), labelled with Carboxy Fluorescein Succinimidyl Ester (CFSE) (5 μM) and used as responders. For suppression assays, the CSFE-labeled CD4+CD25– responders (1×10^4 cells) were stimulated for 72 h in 96-well round-bottom plates with mitomycin C treated splenocytes (1×10^4 cells) and anti-CD3 mAb. WT FOXP3 or DSM FOXP3 transduced cells were used as suppressors and co-cultured with the responders at the indicated ratios. Proliferation of the responders was monitored as a function of CSFE dye dilution.

EMSA assays

EMSA assays to detect ability of the FOXP3 mutants to bind DNA were performed as previously described (Koh et al., 2009). Briefly, single-stranded oligonucleotides containing the consensus Foxp1/FOXP3 binding sites (one strand shown with putative binding sites underlined: 5'-CAAGGTAAACAAGAGTAAACAAGTC-3') were annealed with their complementary strands and purified on 12% polyacrylamide gels for use as probes in electrophoretic mobility-shift assays (EMSA). Probes were end-labeled with γ^{32}P-ATP using T4 polynucleotide kinase in accordance with manufacturers' instructions. In vitro-translated proteins were generated using the TNT reticulocyte lysate system (Promega). Binding reactions were performed at room temperature for 20 minutes using 5 μl of in vitro-translated proteins and approximately ~0.1-0.5 ng (~10,000-20,000 cpm) of ^{32}P-end labeled probes in 20 μl. The final concentration of components of the binding buffer for all EMSA experiments were: 12 mM HEPES pH 7.5, 100 mM NaCl, 1 mM DTT, 1mM EDTA, 12% glycerol and 20 μg/ml poly(dI)-poly(dC). DNA-protein complexes were separated from free probe by electrophoresis in a 5% polyacrylamide, TBE gel containing 1% glycerol. Dried gels were exposed to autoradiography film between 7 hours – overnight at room temperature.

Western blot

Equal quantities of in vitro translated protein lysates were resolved by SDS polyacrylamide gel electrophoresis and transferred to nitrocellulose membranes (Whatman). Immunoblots were performed using either a monoclonal antibody against full-length human FOXP3 (generously provided by Dr. Steven Ziegler). Antibodies were diluted in Tris-buffered saline containing 0.1% Tween-20 and 3% non-fat dry milk. Secondary horseradish peroxidase conjugated goat anti-mouse or anti-rabbit secondary antibodies (Sigma-Aldrich) were used to detect primary antibody binding, followed by detection with an enhanced chemiluminescence

Induction of diabetes

CD4+ T cells were isolated from BDC2.5/NOD mice, activated under Th1 conditions (Ansel et al., 2004), and infected as described above with MSCV IRES-Thy1.1 retrovirus, empty or encoding WT or DSM FOXP3. Three days after infection, Thy1.1+ cells were sorted and transferred into neonatal NOD mice at a 1:2 ratio (0.5×10^5: 1×10^5) with untransduced BDC2.5/NOD Th1 cells ("effector" cells).

Recipient mice were monitored for diabetes (urinary glucose more than 300 mg/dl in two consecutive measurements) for 6 weeks.

Microarray analysis
CD4+CD25- T cells were purified from BDC2.5 TCR transgenic mice and activated with plate bound anti-CD3 and anti-CD28 antibodies. 16 hours after activation the cells retrovirally transduced with MSCV IRES-Thy1.1 retrovirus, empty or encoding WT or DSM FOXP3. 48 hours after initial activation, the cells were removed from the anti-CD3 and anti-CD28 coated plates and expanded with 100 units/ml of recombinant human IL-2 for an additional 3 days. Transduced cells were identified and sorted based on Thy1.1 expression. RNA was extracted from the cells immediately after sorting or after 4 hours of activation with PMA (10 nM) and Ionomycin (1 μM). RNA was extracted using the Trizol reagent (Invitrogen) and amplified for two rounds using the MessageAmp amplified RNA kit (Ambion). The amplified RNA was subsequently labeled with the BioArray High Yield RNA Transcription Labeling Kit (Enzo Diagnostics) and purified with the RNeasy Mini Kit (Qiagen). The resulting cRNAs (two independent data sets for each sample type) were hybridized to Mouse Gene 1.0 ST Arrays (Affymetrix) according to the manufacturer's protocol. The initial reads were processed through Affymetrix software to obtain raw .cel files. The microarray data were background-corrected and normalized with the robust multichip analysis algorithm implemented in the GenePattern software package (Reich et al., 2006), and replicates were averaged.

To better visualise the impact of the domain swap mutations, we calculated a “DSM index” for each gene from the averaged expression values (WT-DSM / WT-Empty). The denominator of this index is positive for FOXP3-activated genes, negative for FOXP3-repressed genes, and 0 for genes whose expression was unaffected by FOXP3. As the denominator tends towards zero (i.e. for genes whose expression was only slightly altered by FOXP3), the DSM index tends to infinity in either direction; to minimize this problem, we have omitted genes whose expression was unaltered or only mildly affected by FOXP3 (Figure 5B, *middle section of the graphs*). Thus for genes whose expression was influenced by FOXP3 (i.e. where the denominator is not equal to 0), the DSM index quantifies the fraction of the FOXP3 effect (activation or repression) that depended on domain swapping. For any given gene, a DSM index near 0 indicates that WT FOXP3 and FOXP3-DSM had similar effects, i.e. the DSM mutation did not affect gene expression. In contrast, a DSM index of 1 indicates that the domain swap mutation abrogated the transcriptional effect of FOXP3 for the gene in question: the biological effect of the DSM mutant (numerator) was close to that observed upon transduction of empty vector (denominator). Effects outside these boundaries (i.e. >1 or <0) may be due to dysregulation of endogenous FOXP3, or to the fact that ratios tend to exaggerate any scatter in the data.

Figure S1: Overall structure of the NFAT1:FOXP3:DNA complex
Complexes containing two NFAT1 DNA-binding domains (RHR-N: yellow and RHR-C: green), FOXP3 forkhead domain dimers (red and cyan), and DNA (stick model) are bridged together by the domain-swapped FOXP dimer in the crystal.

Figure S2: DNA binding by the domain-swapped FOXP3 dimer. (A) Detailed DNA-binding interactions by FOXP3 at Site B, residues are colored and labeled according to proteins. Dashed grey lines denote hydrogen bonds. **(B)** Detailed DNA-binding interactions by FOXP3 at Site A. The cis-monomer binds Site B of one DNA (underlined: 5’-TGGAAAATTTGTTTCA- 3’) (Figure 1A, the bottom DNA). The trans-monomer binds a separated DNA molecule at site A (underlined: 5’-TGGAAAATTTGTTTCA-3’) (Figure 1A, the upper DNA). The binding of the trans-monomer to site A follows the general mechanism of DNA binding by the forkhead domain (Stroud et al., 2006; Wu et al., 2006). The binding of Site B by the cis-monomer, however, shows some deviations from the

canonical mode. Most notably, the highly conserved Asn383 does not interact with DNA directly whereas Arg386 forms bidendate hydrogen bonds with Gua10. His377 forms a hydrogen bond with the phosphate backbone, whereas its counterpart in the trans-monomer flips into the domain swapped interface to interact with Phe371 of its dimer partner. It is noteworthy that FOXP3 binds DNA through a composite protein surface wherein residues from both monomers jointly recognize DNA.

Figure S3: An additional dimerization interface present exclusively in FOXP3 imparts additional stability to the FOXP3 forkhead dimer.
(A) Comparisons of the structures of the forkhead domains of FOXP2 (*left*) and FOXP3 (*right*). One monomer is coloured in red and the other in cyan. The dimerization interface formed by the H2 helices of the two monomers is present in both FOXP2 and FOXP3. In contrast the H1 helices are angled away from each other in FOXP2, making the H1 dimerization interface unique to FOXP3. The presence of this additional dimerization interface may provide a structural explanation of the SEC-MALS data shown in the bottom panel. **(B)** While the forkhead domain of FOXP2 exists as a mixture of monomers and dimers (*left*), the FOXP3 forkhead domain is present exclusively as a dimer (*right*; the FOXP2 A539P mutant, which exists exclusively as a monomer, is shown as a reference). The MALS data in the bottom left panel are from (Stroud et al., 2006) whereas the MALS data in the bottom right panel are from Figure 3b of this article and are reproduced here for ease of direct comparison.

Figure S4: Domain Swap Mutations do not affect Foxp3 expression. Expression of WT and DSM FOXP3 evaluated by flow cytometry. Cells were transduced with bicistronic retroviruses encoding the indicated *FOXP3* constructs and GFP expression was driven by an IRES element. Thus GFP fluorescence is representative of retrovirally expressed mRNA levels. Actual FOXP3 levels in the transduced cells were determined using intracellular staining. As GFP fluorescence and the intensity of FOXP3 staining is the same for both WT and DSM FOXP3, it would denote similar steady state levels. Under conditions where protein synthetic rates are equivalent, flow cytometry provides an accurate index of protein degradation rates (Banaszynski et al., 2006; Iwamoto et al.); thus our data also imply that WT and DSM FOXP3 proteins have very similar stabilities, since both are expressed from the same retroviral promoter.

Figure S5: Repression of select FOXP3 target genes is impaired by DSM mutations.
Relative expression values for the indicated genes obtained by microarray analysis. Expression values obtained from microarray analysis were normalized and expressed relative to cells transduced with empty vector. The data show the mean and range of two independent microarray experiments. The DSM indices for these genes are depicted in Figures 5A and 5B.

Figure S6: Equal proportions of WT and DSM transduced cells are present in recipient NOD mice. Representative FACS plots and bar graphs (mean $\pm$ SEM for 3 individual recipient mice) of splenocytes from recipient BDC2.5 TCR transgenic NOD mice injected nine days previously with BDC2.5 Th1 cells retrovirally transduced to express DSM or WT FOXP3 as well as Thy1.1+. The proportions of Thy1.1+ DSM and WT FOXP3 transferred cells are equivalent, indicating that cells transduced with FOXP3 DSM mutant were not compromised for survival.

Figure S7: Overexpression of affected genes individually is not sufficient to restore the suppressor functions of IPEX mutants. (A) Expression of indicated FOXP3 target genes in WT and F373A transduced T cells as estimated by real-time PCR analysis. Error bars represent the SD observed in three independent experiments. (B) The defect in induction of suppressor function by FOXP3-F373A is not restored by overexpression of indicated genes. Representative histograms depicting the CFSE dilution profile of responder cells cultured T cells transduced FOXP3-WT, FOXP3-F373A or FOXP3-F373A+Cyp11a1 (*Top)* or or FOXP3-F373A+TIGIT (suppressors) at a ratio of 1:2 (suppressors:respondors). *Right;* graphs demonstrating relative proliferation of responder cells

cultured with transduced FOXP3-expressing suppressor cells at different suppressor:respondor ratios. The data are representative of two independent experiments.

References:

Ansel, K.M., Greenwald, R.J., Agarwal, S., Bassing, C.H., Monticelli, S., Interlandi, J., Djuretic, I.M., Lee, D.U., Sharpe, A.H., Alt, F.W., and Rao, A. (2004). Deletion of a conserved Il4 silencer impairs T helper type 1-mediated immunity. Nat. Immunol. *5*, 1251-1259.

Banaszynski, L.A., Chen, L.C., Maynard-Smith, L.A., Ooi, A.G., and Wandless, T.J. (2006). A rapid, reversible, and tunable method to regulate protein function in living cells using synthetic small molecules. Cell *126*, 995-1004.

Brunger, A.T., Adams, P.D., Clore, G.M., DeLano, W.L., Gros, P., Grosse-Kunstleve, R.W., Jiang, J.S., Kuszewski, J., Nilges, M., Pannu, N.S.*, et al.* (1998). Crystallography & NMR system: A new software suite for macromolecular structure determination. Acta Crystallographica *54*, 905-921.

Carson, M. (1991). Ribbons 2.0. J. Appl. Crystallogr. *24*, 958-961.

Iwamoto, M., Bjorklund, T., Lundberg, C., Kirik, D., and Wandless, T.J. (2010). A general chemical method to regulate protein stability in the mammalian central nervous system. Chem Biol *17*, 981-988.

Jones, T.A., Zou, J.Y., Cowan, S.W., and Kjeldgaard, M. (1991). Improved methods for building protein models in electron density maps and the location of errors in these models. Acta. Crystallogr. A *47 (Pt 2)*, 110-119.

Kraulis, P.J. (1991). MOLSCRIPT: a program to produce both detailed and schematic plots of protein structures. J. Appl. Crystallogr. *24*, 946-950.

Otwinowski, Z., and Minor, W. (1997). Processing of X-ray Diffraction Data Collected in Oscillation Mode. Methods in Enzymology *276*, 307-276.

Reich, M., Liefeld, T., Gould, J., Lerner, J., Tamayo, P., and Mesirov, J.P. (2006). GenePattern 2.0. Nat. Genet. *38*, 500-501.

Supplemental Figure-1

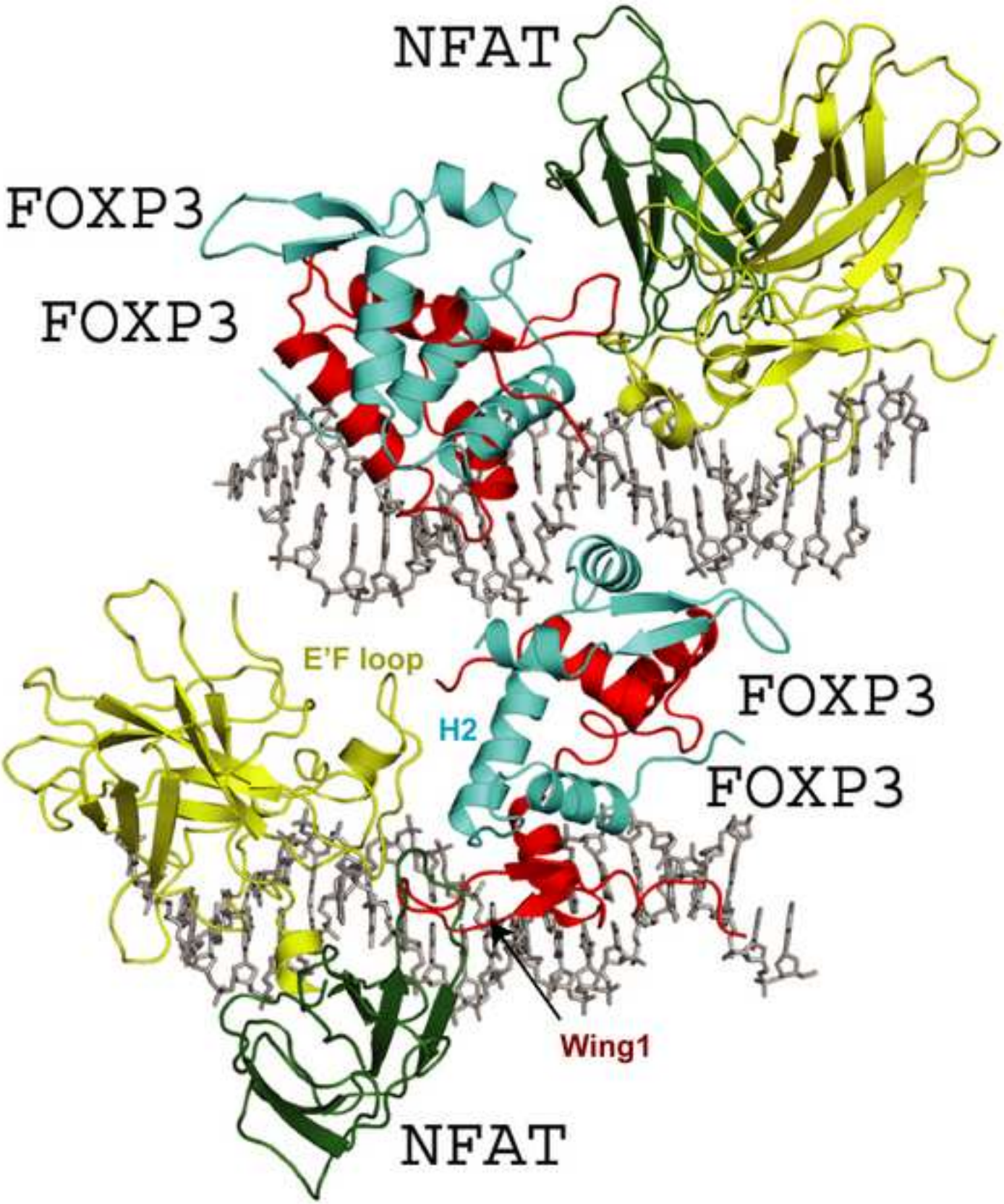

Supplemental Figure-2

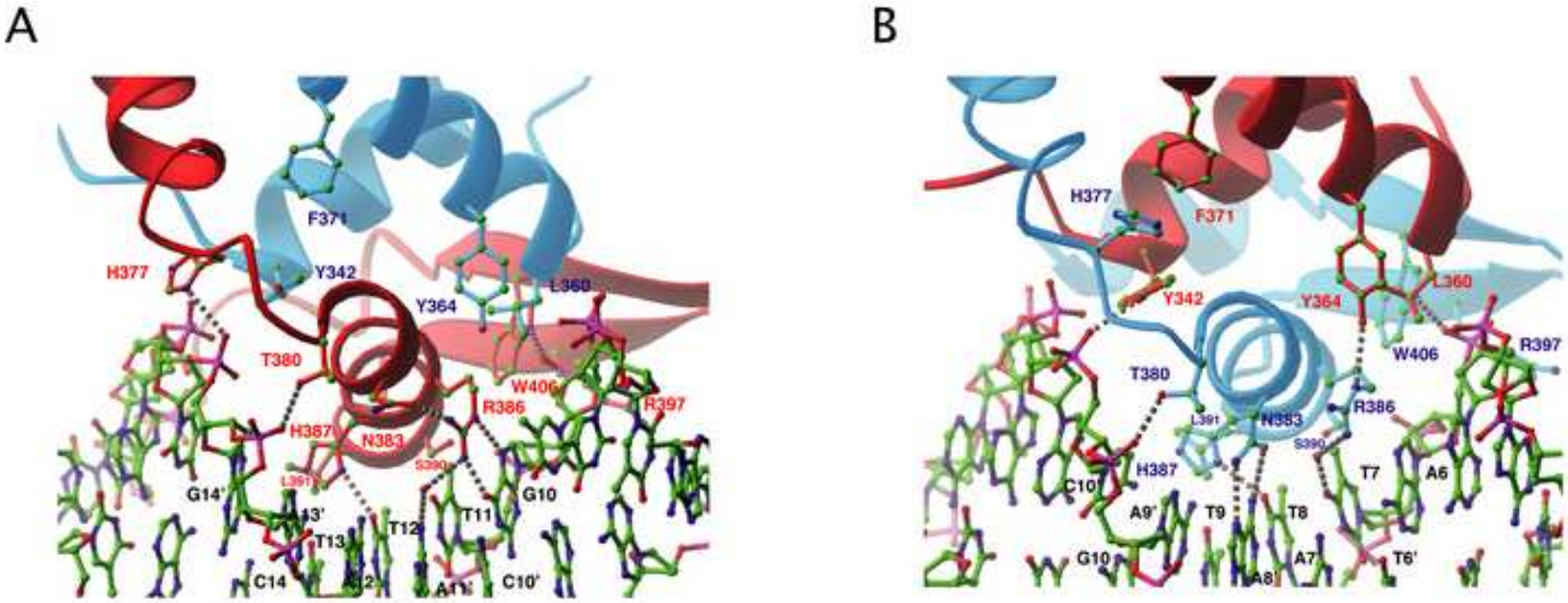

Supplemental Figure-3

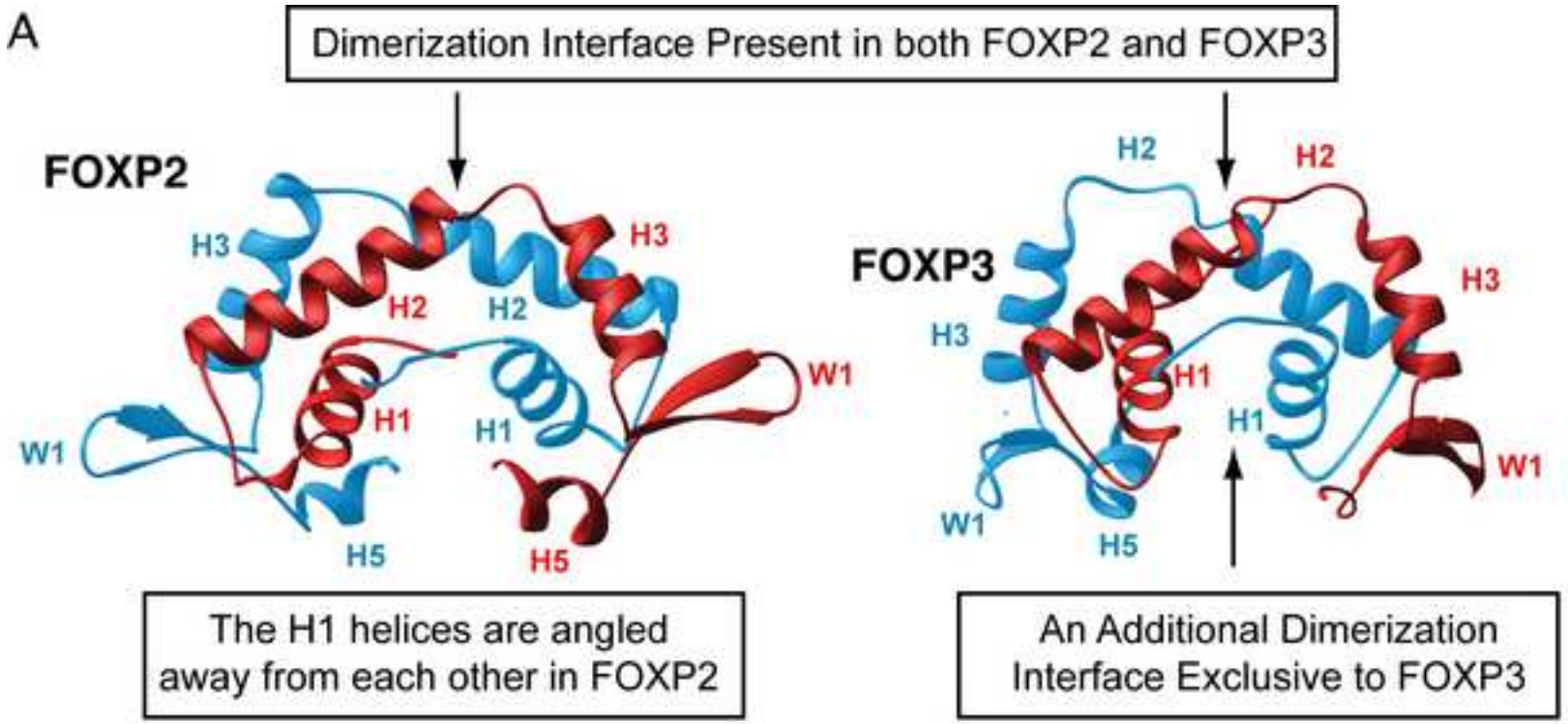

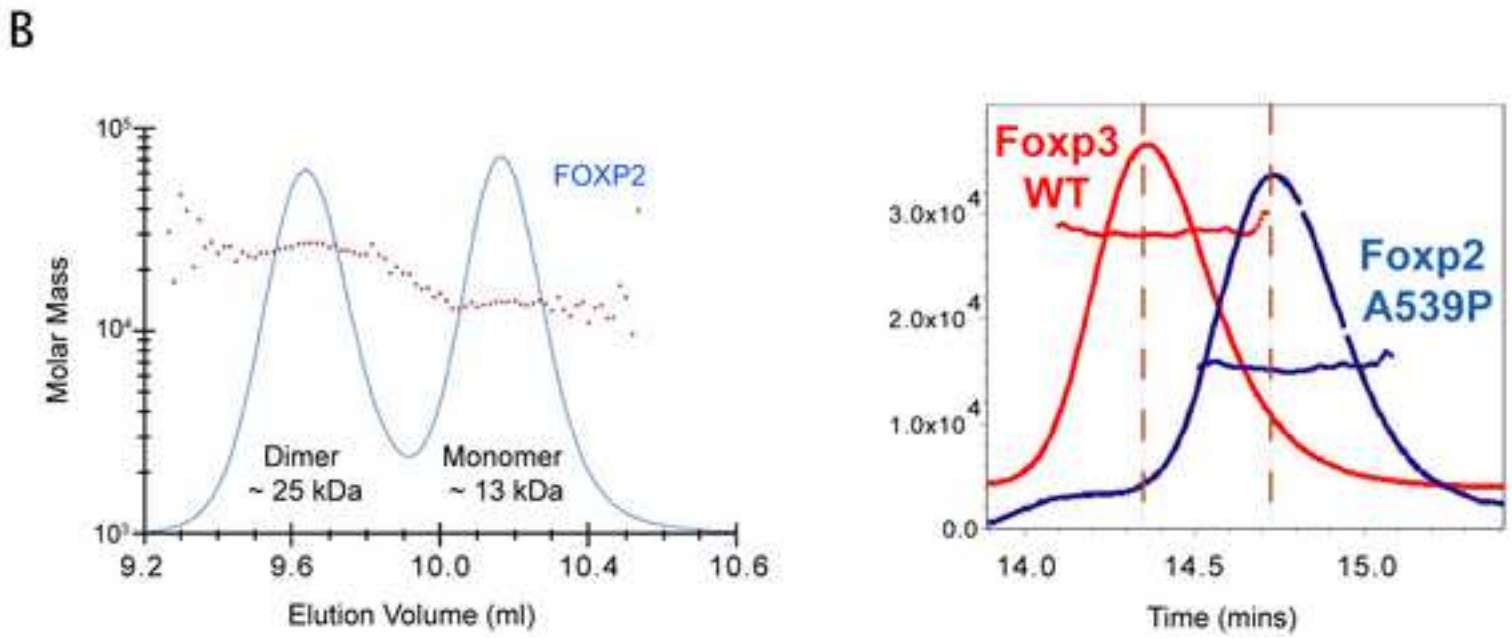

Supplemental Figure-4

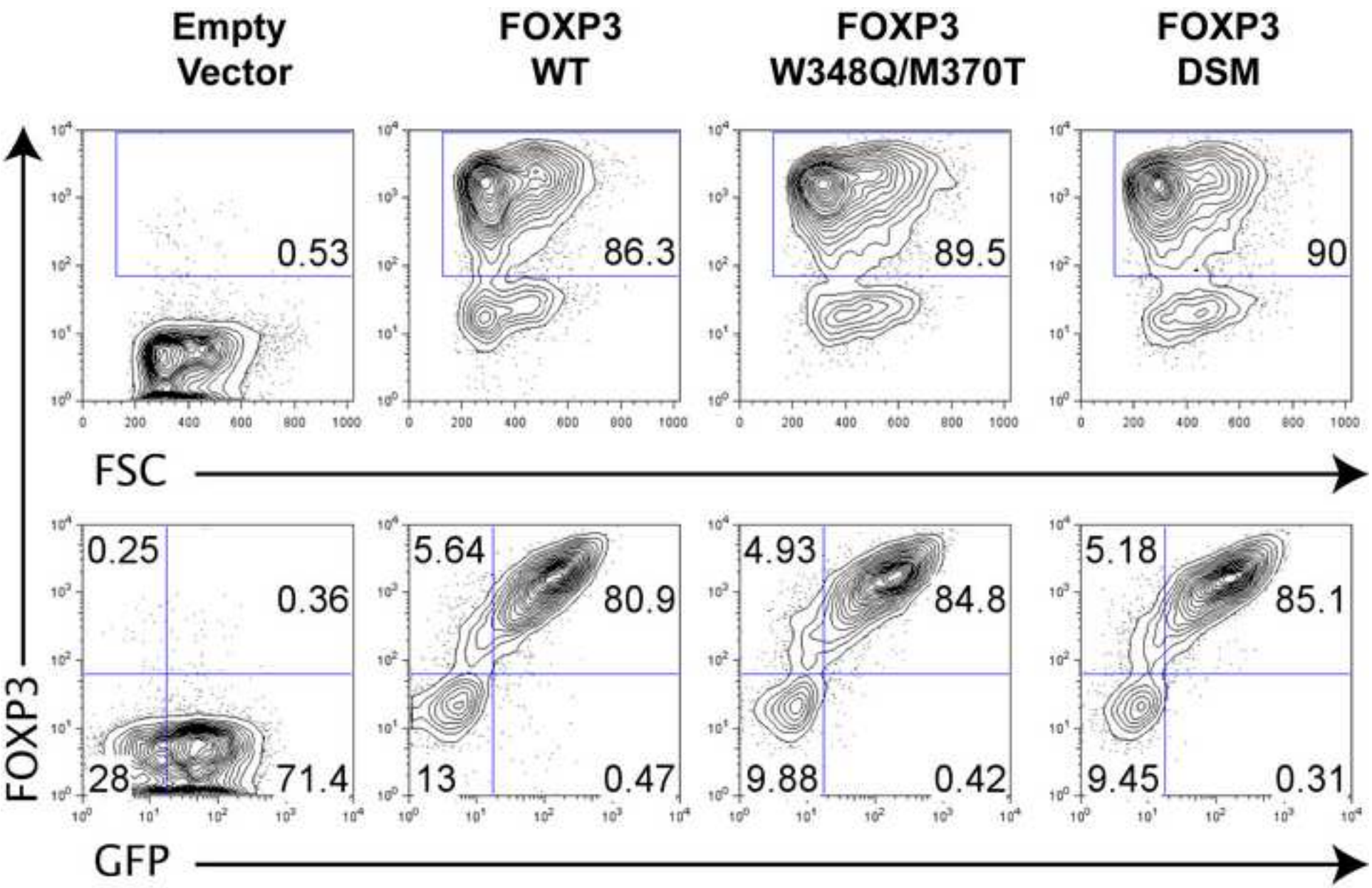

Supplemental Figure-5

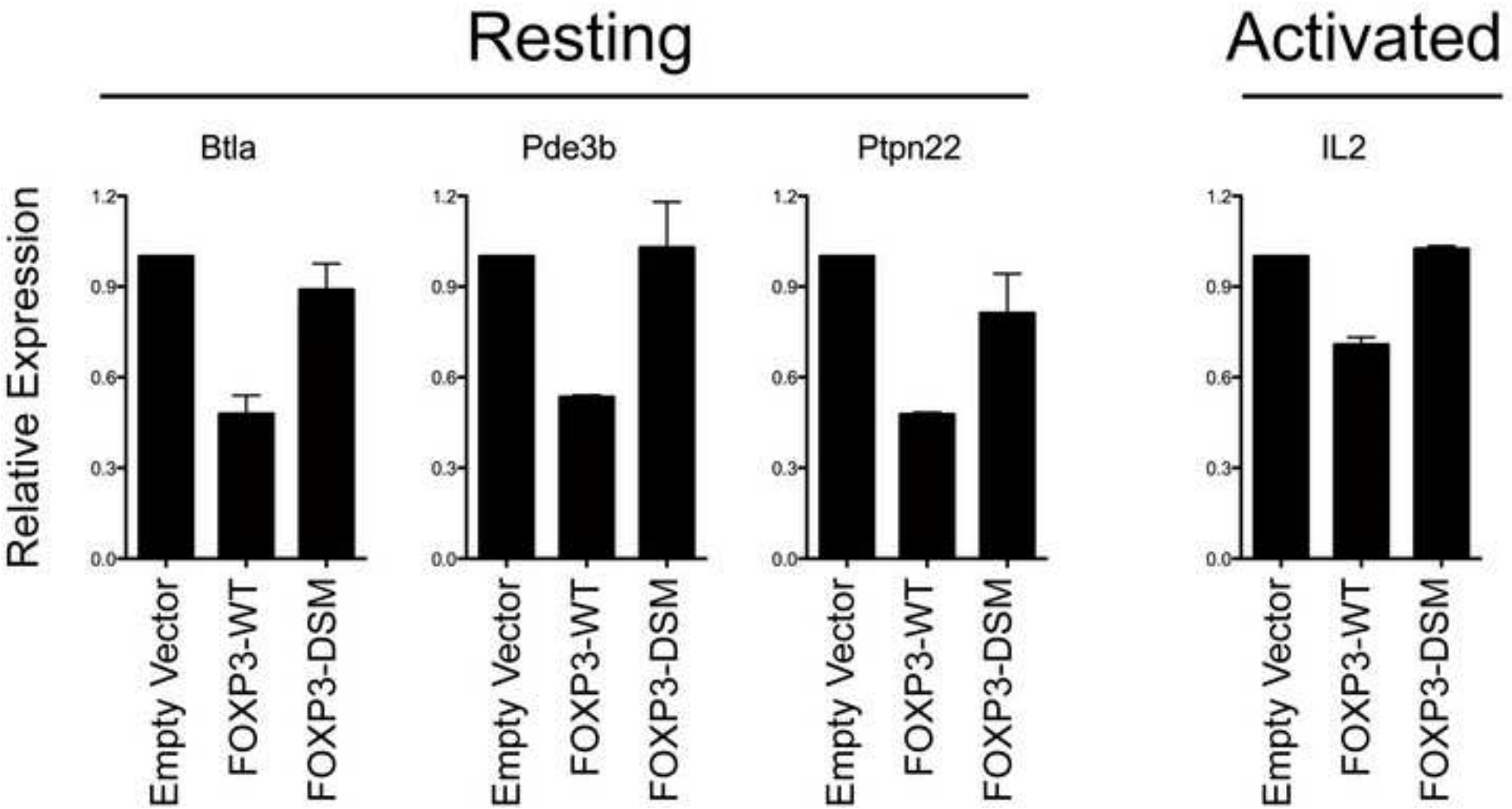

Supplemental Figure-6

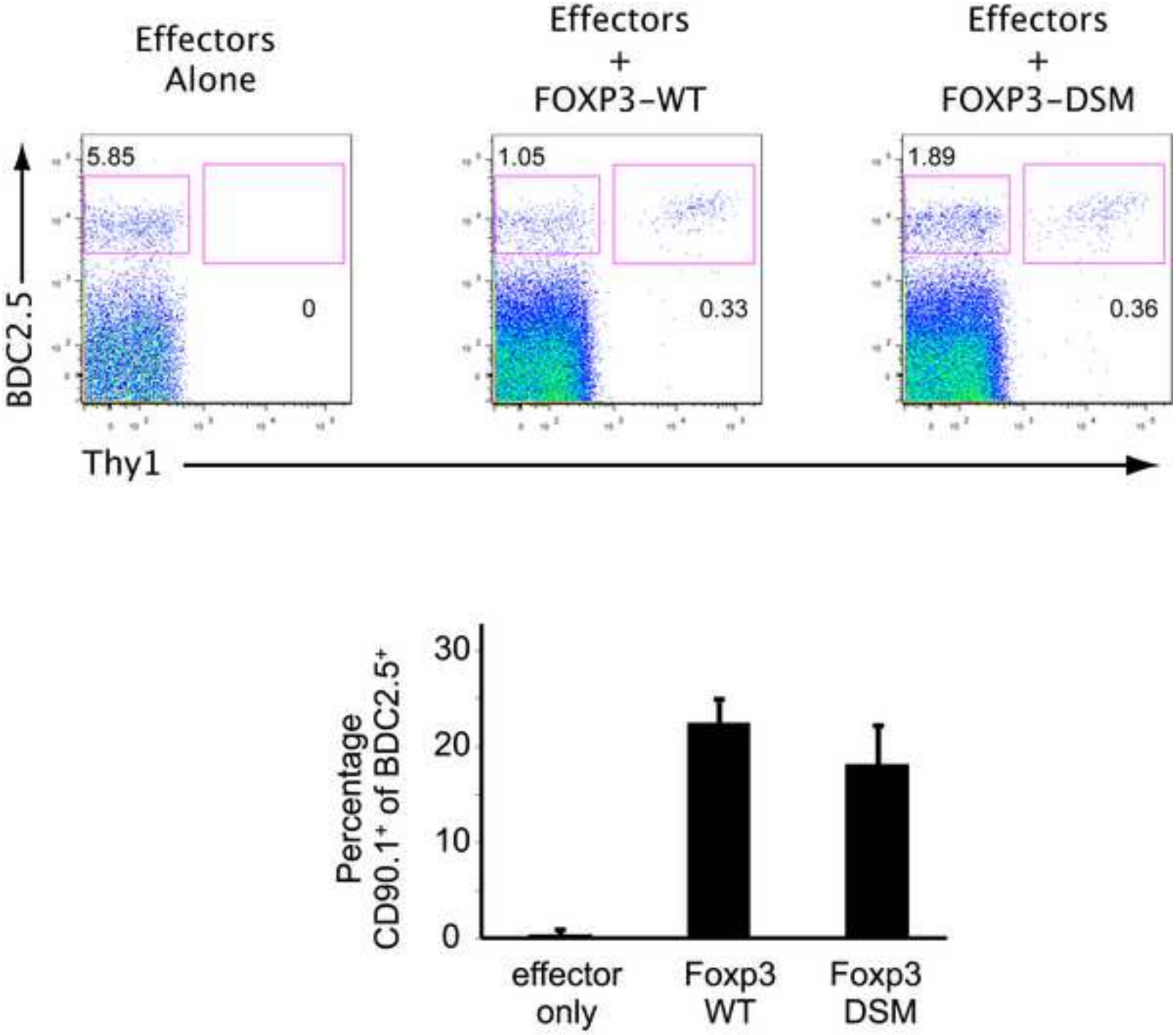

Supplemental Figure-7